Magnetic background noise cancellation in real-world environments

P. J. M. Wöltgens, and R. H. Koch

Citation: Review of Scientific Instruments **71**, 1529 (2000);
View online: https://doi.org/10.1063/1.1150490
View Table of Contents: http://aip.scitation.org/toc/rsi/71/3
Published by the American Institute of Physics

Magnetic background noise cancellation in real-world environments

P. J. M. Wöltgens[a] and R. H. Koch
IBM T. J. Watson Research Center, Yorktown Heights, New York 10598

(Received 23 February 1999; accepted for publication 5 November 1999)

Measurements of the magnetic field noise and the spatial correlation of the noise were made in a typical laboratory environment using two three-axis fluxgate magnetometers. The magnitude of the magnetic field noise was found to be approximately 100 pT/$\sqrt{\text{Hz}}$ at 10 Hz with a correlation of 90% at a separation of 1 m between the two sensors. The correlation was significantly reduced from noise induced eddy currents near large metallic surfaces. © *2000 American Institute of Physics.* [S0034-6748(00)02103-1]

I. INTRODUCTION

Measurements of small magnetic fields at low frequencies (<100 Hz) have promising applications in the medical field, such as magnetoencephalography and magnetocardiography.[1–4] So far, magnetically shielded rooms have been required for most such biomagnetic measurements in order to shield the magnetic background noise of a typical laboratory environment from the measurement. The high costs of these shielded rooms have limited the use of these systems to a few laboratories. Biomagnetic applications would potentially gain in popularity if the necessity of magnetic shielding could be reduced or completely eliminated. In order to achieve this, the magnetic background noise needs to be *cancelled* instead of *shielded* from the measurement. Thus, noise cancellation is an important issue for biomagnetism. In this article a systematic investigation will be presented on magnetic background noise and its cancellation in a laboratory environment.

Background noise cancellation is based on the use of a signal sensor and one or more reference sensors. The signal sensor is positioned in such a way that it measures as much as possible of the signal of interest, superimposed on the unavoidable environmental background noise. The reference sensors are arranged such that they measure as little as possible of the signal of interest while measuring a background resembling as closely as possible the background noise at the signal sensor. The background noise in the signal channel is then estimated on the basis of the reference signals B_{ref}. The estimated signal of interest B_{corr} is then obtained by removing the estimated background noise B_{back} from the measured signal B_{sig}. This subtraction or cancellation can be performed actively or passively: actively, by cancelling the physical quantity B_{back} at the input of the signal sensor[5] and passively, by subtracting B_{back} after the output of the signal sensor.[6,7]

In a real-world environment there are many different background sources at different locations and therefore the magnetic background at each point in space consists of a different mix of fields from these background sources. This is a basic dilemma in noise cancellation: how to locate the reference sensor with respect to the signal sensor. On one hand, the reference sensor should be as close as possible to the signal sensor in order to measure the same background as the signal sensor; on the other hand, the reference sensor should be far away from the signal sensor, so that it measures as little as possible of the signal of interest.

This is the major question this article tries to answer: to what extent is the background constant as a function of position, i.e., how far away from each other can the signal and reference sensors be in order to obtain a certain background rejection?

In this article, first a comparison will be made of a few methods of cancellation. The coherence is identified as the quantity ruling the degree of cancellation, and based on this the feasible amount of cancellation is investigated as a function of the distance between a signal sensor and its reference. Finally, the influence of close-by conductors on magnetic background cancellation will be discussed.

II. CANCELLATION METHODS

The methods which were investigated and will be discussed below are (in order of increasing complexity): (i) subtraction, (ii) balancing in the time domain, and (iii) balancing in the frequency domain.

A. Subtraction

The simplest way of cancellation is subtraction of the reference channel B_{ref} from the signal channel B_{sig}, as is done in the measurement of a gradient, i.e., using the reference B_{ref} as the estimate for the noise in the signal channel

$$B_{\text{back}}(t) = B_{\text{ref}}(t). \tag{1}$$

B. Linear regression fit in the time domain

A more sophisticated way to estimate the noise in the signal channel is to make a linear regression fit in the time domain of the signal channel B_{sig} with respect to the reference channels $B_{\text{ref},j}$. This will result in an estimate for the noise in the signal channel B_{back}:

$$B_{\text{back}}(t) = \sum_j a_j B_{\text{ref},j}(t), \tag{2}$$

where the coefficients a_j are the (time independent) fit coefficients of the regression fit.

[a]Electronic mail: woelt@us.ibm.com

The values of the coefficients are chosen such that the standard deviation of $B_{\mathrm{sig}}(t)$ with respect to $B_{\mathrm{back}}(t)$ is minimized, by setting

$$\frac{\partial}{\partial a_i}\sum_t [B_{\mathrm{sig}}(t)-B_{\mathrm{back}}(t)]^2=0 \tag{3}$$

for all i. In matrix notation this can be expressed as

$$\mathbf{b}=\mathbf{\Gamma a}, \tag{4}$$

where $\mathbf{b}$ is a vector with components

$$b_i=\sum_t [B_{\mathrm{sig}}(t)B_{\mathrm{ref},i}(t)], \tag{5}$$

$\mathbf{\Gamma}$ is the symmetric correlation matrix with components

$$\Gamma_{ij}=\sum_t [B_{\mathrm{ref},i}(t)B_{\mathrm{ref},j}(t)], \tag{6}$$

and $\mathbf{a}$ is a vector the components a_j of which are the fit parameters.

The multiple-regression equation is then solved by computing the inverse matrix $\mathbf{\Gamma}^{-1}$ of $\mathbf{\Gamma}$ and evaluating

$$\mathbf{a}=\mathbf{\Gamma}^{-1}\mathbf{b}. \tag{7}$$

C. Linear regression fit in the frequency domain

A more refined way of cancellation is to do a linear regression fit in the frequency domain. (See Ref. 8.) Such a fit results in an estimate for the noise in the signal channel $B_{\mathrm{back}}(f)$ according to

$$B_{\mathrm{back}}(f)=\sum_j H_j(f)B_{\mathrm{ref},j}(f), \tag{8}$$

where the transfer functions $H_j(f)$ are the optimum frequency response functions, the results of the linear regression fit. These functions $H_j(f)$ are chosen such that the spectral density of $B_{\mathrm{back}}(f)-B_{\mathrm{sig}}(f)=B_c(f)$ is minimized, i.e.,

$$\frac{\partial S_{\mathrm{cc}}(f)}{\partial H_i(f)}=0 \quad \text{and} \quad \frac{\partial S_{\mathrm{cc}}(f)}{\partial H_i^*(f)}=0 \tag{9}$$

for all i, with $S_{\mathrm{cc}}(f)$ the power-spectral density of B_c and $H_i^*(f)$ the complex conjugate of $H_i(f)$. Again, this minimization can be expressed in terms of a matrix equation

$$\mathbf{s}=\mathbf{\Gamma}_f\mathbf{h}, \tag{10}$$

where $\mathbf{s}$ is a vector with components

$$s_j=S_{j,\mathrm{sig}}(f). \tag{11}$$

Here, $S_{j,\mathrm{sig}}(f)$ is the cross-spectral density of $B_{\mathrm{ref},j}(t)$ and $B_{\mathrm{sig}}(t)$. Further, $\mathbf{\Gamma}_f$ is a Hermitian matrix with components

$$\Gamma_{f,ij}=S_{ij}(f) \tag{12}$$

with $S_{ij}(f)$ the cross-spectral density of $B_{\mathrm{ref},i}(t)$ and $B_{\mathrm{ref},j}(t)$. Finally, $\mathbf{h}$ is a vector with components

$$h_j=H_j(f). \tag{13}$$

Analogously to the time-balanced case, the solution for $\mathbf{h}$ can be found by inversion of $\mathbf{\Gamma}_f$.

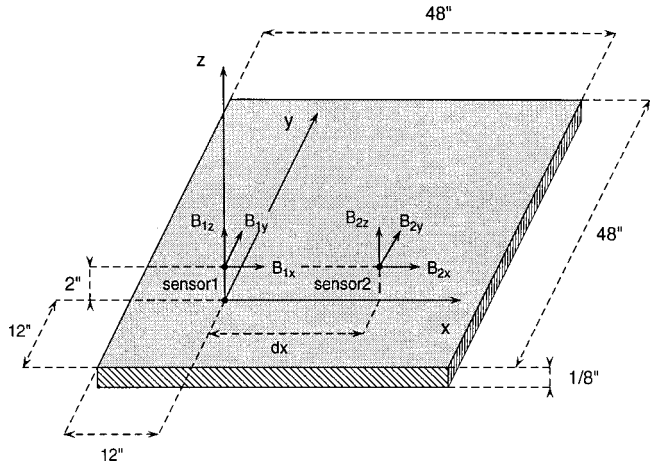

FIG. 1. The setup for coherence/cancellation measurements in a laboratory environment.

III. EXPERIMENTAL SETUP

To investigate the magnetic background noise in a laboratory and its cancellation, we measured the noise simultaneously at two locations in our laboratory, using a setup as depicted in Fig. 1. For magnetic sensors we used two Billingsley TFM100-RLN three-axis fluxgate magnetometers with a noise level of $10-15\,\mathrm{pT}/\sqrt{\mathrm{Hz}}$ in the frequency range of 0.1–100 Hz. The sensors were placed in our lab on a horizontal plate of dimensions 48 in.×48 in. (1.22 m×1.22 m). One sensor (sensor 1) remained in a fixed position, while the position of the other sensor (sensor 2) was varied along two perpendicular directions parallel to the edges of the plate designated the x axis and y axis. Both sensors were located 2 in. (0.051 m) above the platform surface. The sensors were oriented parallel to each other to within less than 0.03 rad, and the x, y, and z channels of each three-axis fluxgate were orthogonal to better than 0.017 rad. We varied the height of the plate above the floor and the material of the plate, comparing nonconductive (wooden) plates and conductive plates [1/8 in. (3.18 mm) thick, made of aluminum and nonstainless steel]. Further, we moved the whole setup to an adjacent lab in order to test reproducibility of our results. The x, y, and z signals of both sensors were filtered via 120 Hz low-pass filters with a roll-off of -24 dB/octave. The filter outputs were subsequently digitized and processed on a personal computer. The time traces were taken during 14 s with a sampling rate of 600 Hz. For spectral analysis we used the average of the spectral estimates of 15 half overlapping, 1.7 s long subdivisions of the main time trace.

IV. MAGNETIC BACKGROUND

We tested the previously described three ways of cancellation using our setup with a large separation (0.60 m) in the x direction between the two fluxgate sensors on a wooden plate. The results are presented in Fig. 2.

The background spectrum in Fig. 2 is typical for a laboratory: at frequencies below 1 Hz the power spectral density has a $1/f^2$ frequency dependence, which is associated with random switching noise with a characteristic frequency below our frequency window. Between 1 and 60 Hz the spec-

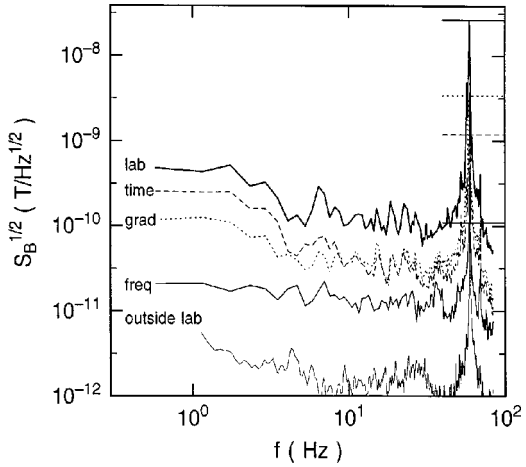

FIG. 2. Magnetic background spectrum and cancellation spectra of this spectrum in an unshielded laboratory environment. Fluxgate sensors 1 and 2 are placed on a wooden platform, separated by a distance of 24.0 in. (0.61 m) in the x direction. The thick solid line is the magnetic background spectrum of B_{1x}. The dotted line is the gradient signal $B_{1x}-B_{2x}$, the dashed line is the time-balanced spectrum of B_{1x} with respect to B_{2x}, B_{2y}, and B_{2z}. The thin solid line is the frequency balanced spectrum of B_{1x} with respect to B_{2x}, B_{2y}, and B_{2z}. The solid, dashed, and dotted horizontal lines indicate the levels of the 60 Hz peaks in the corresponding spectra. The thinnest solid line denotes the magnetic background spectrum outside the laboratory building, as measured with a SQUID magnetometer.

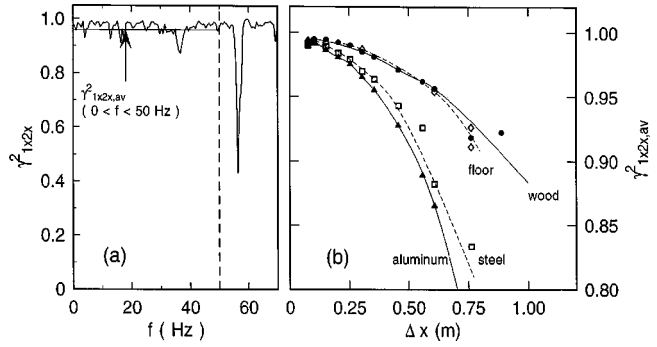

FIG. 3. (a) The way the averaged coherence between 0 and 50 Hz is determined. (b) The averaged coherence $\gamma^2_{1x2x,\mathrm{av}}$ between B_{1x} and B_{2x} as a function of the distance between sensor 2 and sensor 1 in the x direction. The labels indicate the different plate materials for which the results were obtained.

trum is roughly flat, with an average level of about $100\,\mathrm{pT}/\sqrt{\mathrm{Hz}}$. This white noise below 60 Hz has been observed by other groups[1,4] in laboratory environments, but its origin is as yet unknown. At 60 Hz, the magnetic field from the power line has a level of $60\,000\,\mathrm{pT}/\sqrt{\mathrm{Hz}}$ or $46\,000\,\mathrm{pT_{rms}}$. As a reference, Fig. 2 also shows a magnetic background spectrum taken outside the laboratory building using a superconducting quantum interference device (SQUID) magnetometer. A comparison with the noise spectrum taken in the laboratory shows that the white magnetic laboratory noise below 60 Hz is associated with the laboratory building and not with geomagnetic noise.

V. CANCELLATION RESULTS

Figure 2 further shows the cancellation spectra resulting from the cancellation methods discussed in the previous subsection. Taking the gradient reduces the overall background noise by a factor of four and the 60 Hz line peak by a factor of 7.

At the expense of a small increase in the noise at frequencies below 5 Hz, time balancing reduces the 60 Hz peak by a factor of 22. The balancing of B_{1x} with respect not only to B_{2x}, but also to the orthogonal components B_{2y} and B_{2z} eliminates noise due to a misalignment of the sensors with respect to each other. Apparently, the noise decrease at 60 Hz in the balanced spectrum outweighs the noise increase at lower frequencies.

Finally, B_{1x} was balanced in the frequency domain with respect to B_{2x}, B_{2y}, and B_{2z}. This form of cancellation provided the best background noise rejection: at frequencies below 60 Hz a reduction of about 14× and at 60 Hz a reduction of 300×. For frequencies other than 60 Hz, the resulting cancelled noise spectrum is very close to the limit set by the fluxgate noise of $10\,\mathrm{pT}/\sqrt{\mathrm{Hz}}$. The better performance of frequency balancing as compared to the previously described methods can be understood if one realizes that in a real-world environment multiple magnetic source are present, emitting magnetic fields at different frequencies. Thus, at different frequencies the outputs of signal and reference sensors may very well reflect different combinations of magnetic sources and therefore display different correlations.

VI. LIMITS ON CANCELLATION

In the real world, multiple magnetic sources are present, limiting the feasible amount of cancellation between two sensors to finite values. We investigated how these limits depend on the distance between the signal sensor and its reference sensor, using the previously described setup with metallic and nonmetallic plates as measurement platforms. The relevant parameter to characterize the maximum noise reduction is the coherence $\gamma^2_{\mathrm{sig,ref}}$ of a signal B_{sig} and its reference B_{ref}, and is defined as follows:

$$\gamma^2_{\mathrm{sig,ref}}(f)=\frac{|S_{\mathrm{sig,ref}}(f)|^2}{S_{\mathrm{sig}}(f)S_{\mathrm{ref}}(f)}, \tag{14}$$

with $S_{\mathrm{sig,ref}}(f)$ the cross-spectral density between the reference and the signal sensor. Here, $S_{\mathrm{sig}}(f)$ and $S_{\mathrm{ref}}(f)$ are the power-spectral densities of the signal sensor and the reference sensor, respectively. The coherence is thus a normalized cross-spectral density between the two signals, having real values between 0 and 1. The power-spectral density S_{uncorr} of the part of B_{sig} uncorrelated to B_{ref} is then given by

$$S_{\mathrm{uncorr}}=[1-\gamma^2_{\mathrm{sig,ref}}(f)]S_{\mathrm{sig}}. \tag{15}$$

The averaged coherence between 0 and 50 Hz as a function of the sensor–sensor distance is plotted in part (b) of Fig. 3. Qualitatively similar behavior was observed for translations of sensor 2 with respect to sensor 1 in the y direction and for the coherence between y and z channels of the sensors. The exact dropoff of the coherence with distance depends on the circumstances, however, the qualitative behavior of the dropoff remains the same. The upper limit of the coherence, at small sensor–sensor distances, is 0.99: this

limit is set by the sensor noise power of the fluxgate sensors which is about 1/100 of the average background noise power between 0 and 50 Hz. In this two channel analysis, the misalignment between the two sensors can decrease the maximum value of the coherence if they are not aligned to within 10% of each other. The alignment errors in these measurements were less than 10% in the relative alignment. If all three axis were used as references to determine the maximum coherence, any alignment errors would not decrease the maximum value.

In these measurements, as the spacing of the two sensors was increased the coherence decreased. The magnitude of the noise power S_{uncorr} varied as the spacing between the two sensors Δx as $S_{\text{uncorr}} \propto \Delta x^{1.6\pm0.2}$. There is no simple way to understand this particular power law from basic considerations of magnetic sources yet, the general falloff with distance can be understood. The total field noise impinging on both sensors, the main and the reference sensors, consists of contributions from a large number, N, of independent sources. At any one frequency, the complex amplitude ratio of the field on the main sensor and the reference sensor from each of the N sources, $R_j(f)$ (where $j=1,2,3,...,N$) will depend the detailed nature of the source, including its position relative to the main and reference sensors. If there is only one noise source, i.e., $N=1$, than Eq. (8) and a single reference sensor, as used in these measurements, would be able to correct completely for the noise source by adjusting the correlation coefficient $H_1(f)$ to be equal to $R_1(f)$. However, with two or more independent noise sources, the choice of a single value of $H_1(f)$ can only be a compromise. Only in the limit where $\Delta x \to 0$ will all the $R_j(f)$ approach the same value, one, and perfect cancellation be achieved.

Further, a loss of coherence can be observed in the presence of a conductive plate instead of a nonconductive one. This loss occurs in the field directions parallel to the plate, i.e., the x and the y directions, but is absent in the z direction perpendicular to the plate. Using Eq. (15), we can compute the maximum achievable noise amplitude reduction from the coherence between B_{sig} and B_{ref}:

$$\text{maximum reduction} = 1/\sqrt{1-\gamma^2_{1x2x,\text{av}}}. \tag{16}$$

The resulting maximum achievable background noise reduction computed from the data presented in Fig. 3 is plotted in Fig. 4.

The results indicate that in a two-sensor configuration the maximum achievable noise reduction is better than a factor of 10 for separations of less than 0.20 m for frequencies between 0 and 50 Hz. To achieve higher noise rejection factors at these distances, more reference sensors with lower noise levels are necessary. Some of these sensors should be orthogonal to the direction of interest such as to compensate for the misalignment between the sensors.

VII. DEGRADATION OF COHERENCE NEAR METAL

The observed loss of coherence in the magnetic field parallel to a conductive plate can be explained by taking into account electromagnetic induction.

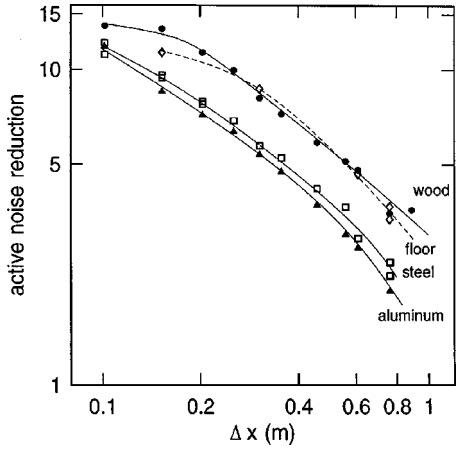

FIG. 4. The averaged reduction computed from the average coherence $\gamma^2_{1x2x,\text{av}}$ of Fig. 3 between the x channels of the two fluxgate sensors as a function of the separation of sensors 1 and 2 in the x direction. The labels indicate the different plate materials for which the results were obtained.

To get a first-order estimate of these inductive effects we perform the following analysis: consider a circular conductive plate radius R and thickness θ in an homogeneous applied magnetic field $\mathbf{B}_a$. The direction perpendicular to the plate is designated the z axis, the x and y axes are orthogonal directions in the plane of the plate. $\mathbf{B}_a$ has a z component $B_{a,z}=B_0 e^{i\omega t}$, where ω is the angular frequency. We consider the limit in which the induced magnetic field B_{ind} is small in comparison to the applied alternating current field B_a. The magnitude of the induced current density J_{ind} at a distance r from the center of the plate is then given by

$$J_{\text{ind}}(r) \propto \frac{i\omega B_{a,z} r}{2\rho}, \tag{17}$$

with ρ the resistivity of the plate.

At a distance $d \ll R$ from the surface of the plate such local eddy currents J_{ind} resemble infinitely long line currents inducing a magnetic field which drops off as $1/d$. Using Ampere's law, it can be shown that the z component of the

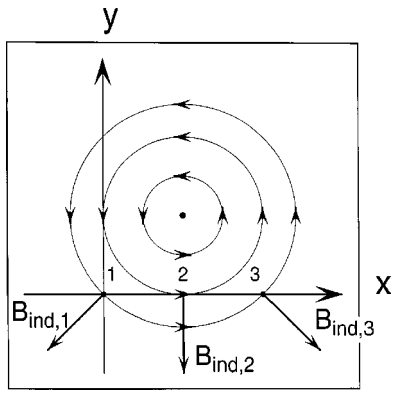

FIG. 5. Illustration of the changes in direction of the in-plane component of the local B_{ind} on the topside of the plate as a function of the position on the x axis. The circles indicate the local eddy current paths, and the vectors $B_{\text{ind},1}$, $B_{\text{ind},2}$, and $B_{\text{ind},3}$ indicate the magnetic field induced on the topside of the plate by these local eddy currents at positions 1, 2, and 3. Note the opposite values of x component of B_{ind} in positions 1 and 3, whereas the y component of B_{ind} changes only by a factor of $2^{1/2}$ from position 2 to positions 1 and 3.

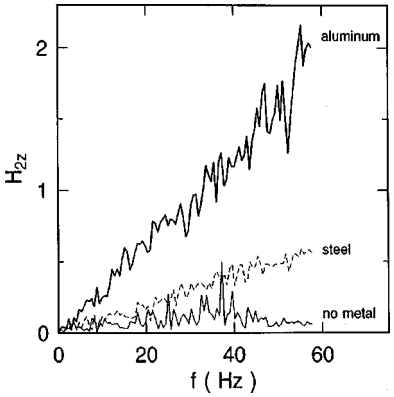

FIG. 6. The frequency dependence of the transfer function H_{2z} of B_{2z} to B_{1x} as obtained from the frequency-dependent balancing of B_{1x} with respect to B_{2x}, B_{2y}, and B_{2z}. Sensor 2 is positioned on the x axis 0.305 m away from sensor 1. Both sensors are located 50.8 mm above the surface of the plate. The thin solid line indicates H_{2z} for a nonconductive plate, the thin dashed line for a steel plate, and the thick solid line indicates H_{2z} for an aluminum plate.

induced field in the center of the plate should scale as: we expect the induced magnetic fields B_{ind} to scale with the induced current density, thus giving

$$B_{\mathrm{ind}}(r) \propto \frac{i\omega B_{a,z} r}{2\rho}. \tag{18}$$

In the rectangular plates used in this experiment, these eddy currents will in first approximation run in concentric circles around the center of the plate as depicted in Fig. 5. Moving along the x axis, the local eddy-current direction rotates, and similarly, the in-plane component of the locally induced magnetic field is rotated. Thus, at different positions along the x axis a sensor measures, in addition to the applied field $\mathbf{B}_a$, a differently directed induced field $\mathbf{B}_{\mathrm{ind}}$. The biggest change occurs in the x component of $\mathbf{B}_{\mathrm{ind}}$, which reverses in direction from position 1 to position 3. The total field at sensor 2 can then, in first approximation, be expressed as: $B_{2x}=B_{1x}+(B_{\mathrm{ind},2x}-B_{\mathrm{ind},1x})$, which means that the coherence loss scales with the magnitude of the local $\mathbf{B}_{\mathrm{ind}}$.

To corroborate this picture, we performed a frequency-dependent multiple regression analysis of B_{1x} vs B_{2x}, B_{2y}, and B_{2z} and computed transfer functions H_{2x}, H_{2y}, and H_{2z}, with sensor 1 located at the origin and sensor 2 positioned somewhere along the x axis. For the case of a nonconductive plate, we trivially find that $H_{2x}=1$, and $H_{2y}=H_{2z}=0$. With a conductive plate, however, the transfer function H_{2z} increases linearly with frequency, while having a frequency-independent phase. Further, a comparison of H_{2z} for different plate materials shows that the magnitude of H_{2z} at a certain frequency drops with increasing resistance of the platform, as is shown in Fig. 6. More quantitatively, at any given frequency H_{2z} is about $4\times$larger for the aluminum plate than for the steel plate, this factor is the same as the conductivity ratio for aluminum and steel ($\rho_{\mathrm{Al}}=2.67\times10^{-8}\,\Omega\,\mathrm{m}$, $\rho_{\mathrm{Fe}}=10.00\times10^{-8}\,\Omega\,\mathrm{m}$).

In general, metallic objects in applied ac magnetic fields will generate induced fields, which effectively mix orthogonal components into each component of the applied magnetic field. As this mix may vary significantly over space the coherence between the magnetic field at two points in space is degraded.

[1] J. Vrba *et al.*, in *Advances in Biomagnetisrn Research: Biomag96*, edited by C. Aine, Y. Okada, G. Stroink, S. Swithenby, and C. Wood (Springer, New York, in press).
[2] J. Vrba, in *SQUID Sensors: Fundamentals, Fabrication, and Applications*, edited by H. Weinstock (Kluwer Academic, Dordrecht, 1996), p. 117.
[3] J. Vrba and J. McKay, Appl. Supercond. **5**, 431 (1997).
[4] H. J. M. ter Brake *et al.*, Inst. Phys. Conf. Ser. **148**, 1503 (1995).
[5] R. H. Koch, J. R. Rozen, J. Z. Sun, and W. J. Gallagher, Appl. Phys. Lett. **63**, 403 (1993).
[6] Y. Tavrin, Y. Zhang, M. Mück, A. I. Braginski, and C. Heiden, IEEE Trans. Appl. Supercond. **3**, 2477 (1993).
[7] J. Borgmann, P. David, G. Ockenfuß, R. Otto, J. Schuber, W. Zander, and A. I. Braginski, Rev. Sci. Instrum. **68**, 2730 (1997).
[8] G. M. Jenkins and D. G. Watts, *Spectral Analysis and its Applications* (Holden-Day, San Francisco, 1968), p. 485ff.